Climate Dynamics (2023) 61:5049–5064
https://doi.org/10.1007/s00382-023-06840-5

Tropical cyclone size asymmetry index and climatology

Kelvin T. F. Chan[1,2,3] **· Kailin Zhang**[1,4] **· Lifeng Xu**[1]

Received: 17 December 2022 / Accepted: 22 May 2023 / Published online: 18 August 2023

Abstract

Size of tropical cyclone (TC) is often asymmetric in nature. Yet, there is a lack of systematic, clean, and intuitive definition/expression to specify the asymmetry of TC size. Here, we introduce a novel index, TC size asymmetry index (SAI), which specifies both the degree and pattern of the asymmetry synthetically. In particular, the symbolic form of SAI is vividly designated for identifying the latter. The SAI proposes 1 quasi-symmetric pattern and 28 asymmetric patterns in total. The 41-year (1979–2019) global climatology of SAI shows that the distribution of the degree of TC size asymmetry is trimodal. Elementarily, the degree and pattern of asymmetry are found to be TC intensity, TC movement, time, and space dependent. The introduction of SAI provides an insight into the subject and lays an important foundation for future applications and research. Furthermore, besides meteorology, it could inspire other fields to index the geometric asymmetries of other kinds.

Keywords Tropical cyclone · Size asymmetry index · SAI · Climatology

1 Introduction

Size of tropical cyclone (TC) is an important metric that specifies how large the influence of a TC is (Chan and Chan 2018). Enhancing the understanding on how the TC size evolves substantially helps the forecast, advisory, and disaster preparedness (e.g., rain, wind, storm surges, storm tides, and tornados; McCaul 1991; Irish et al. 2008; Lin et al. 2014; Paredes et al. 2021; Wang et al. 2022). Most studies defined TC size by taking the azimuthally-averaged radii of particular wind speeds (Chan and Chan 2018). They made use of the best-track data (Kimball and Mulekar 2004; Yuan et al. 2007; Song and Klotzbach 2016; Song et al. 2020), satellite-based observations (Liu and Chan 1999; Dean et al. 2009; Chavas and Emanuel 2010; Knaff et al. 2011, 2014; Chan and Chan 2012, 2015a; Chavas et al. 2016; Klotz and Jiang 2016; Chen et al. 2021; Zhuo and Tan 2021), reanalyses (Liu and Chan 2002; Chan and Chan 2013; Schenkel et al. 2017, 2018; Mok et al. 2018; Bian et al. 2021; Yang et al. 2022), and idealized numerical models (Hill and Lackmann 2009; Xu and Wang 2010a, b; Chan and Chan 2014, 2015b, 2016; Chavas and Emanuel 2014; Wang et al. 2015; Wang and Toumi 2019, 2022; Lu and Chavas 2022) to examine the climatology, characteristics, and possible mechanisms governing the TC size.

Nonetheless, as a matter of fact, the size of TC is often asymmetric or irregular. The surface horizontal circulation of TC can vary remarkably in time and space (Song and Klotzbach 2016; Klotz and Jiang 2016, 2017; Olfateh et al. 2017; Sun et al. 2019; Tamizi et al. 2020). A single azimuthally-averaged value, hence, cannot depict the TC size sufficiently. The research on TC size asymmetry is therefore warranted but limited and inadequate (Olfateh et al. 2017; Sun et al. 2019; Hong et al. 2020). Zhang and Chan (2023) recently evaluated the fidelity of the ERA5 reanalysis data in estimating the outer-core sizes [R34, the radius of 10-m gale-force (34-kt) winds from the TC center] in four cardinal quadrants of TCs. They established a 41-year (1979–2019) global TC size database and exhibited the global climatology. Such a long and homogeneous database lays important groundwork that allows us to study and understand the asymmetry of TC size more possible.

✉ Kelvin T. F. Chan
chenth25@mail.sysu.edu.cn

1 School of Atmospheric Sciences, Sun Yat-sen University, and Southern Marine Science and Engineering Guangdong Laboratory (Zhuhai), Zhuhai, China

2 Guangdong Province Key Laboratory for Climate Change and Natural Disaster Studies, Sun Yat-sen University, Zhuhai, China

3 Key Laboratory of Tropical Atmosphere-Ocean System (Sun Yat-sen University), Ministry of Education, Zhuhai, China

4 Guangdong Piesat Information Technology Co., Ltd., Foshan, China

Notably, although several attempts have been made to define the degree of TC size asymmetry (e.g., Klotz and Jiang 2016; Olfateh et al. 2017; Sun et al. 2019; Hong et al. 2020), they are not generic (not applicable in all circumstances) and not sufficient (no specification on the pattern/shape of TC size asymmetry) enough. This paper, a follow-up of Zhang and Chan (2023), proposes a novel TC size asymmetry index (SAI) to specify the degree and pattern of the asymmetry of TC size in a synthetic way. The introduction of SAI fills the aforementioned deficiencies systematically, which is skillful for interpretation and documentation in applications and research. An elementary global climatology and the power of SAI are revealed and demonstrated stepwise in this study.

2 Data

The global TC size database (Zhang and Chan 2023) inferred from the fifth generation of European Centre for Medium-Range Weather Forecasts (ECMWF) atmospheric reanalysis of the global climate (ERA5; Hersbach et al. 2022) is employed. It is validated by the Quick Scatterometer (QuikSCAT) satellite data. It provides the 41-year (1979–2019) 6-hourly homogeneous estimates of R34 in four cardinal quadrants of TCs over the western North Pacific (WNP), eastern North Pacific (ENP), North Atlantic (NA), South Indian Ocean (SI), and South Pacific (SP). The corresponding elementary best-track data including TC locations, maximum sustained wind speeds (V_{MAX}), and minimum sea-level pressure are also provided. It is noted that although some mainstream best-track data provide sophisticated TC size estimates, they are not employed because of the heterogeneities in operation, estimation, and data availability among different meteorological agencies (Chan and Chan 2012; Chan et al. 2022a, b; Kim et al. 2022).

3 Size asymmetry index (SAI)

Neither the degree nor pattern of asymmetry alone can sufficiently specify the essential asymmetric structure of TC size because they complement each other. In view of this, a novel index, size asymmetry index (SAI), is pertinently introduced and defined as follows.

First, being in line with most of the operational meteorological agencies [e.g., Japan Meteorological Agency (JMA), China Meteorological Administration (CMA), and Joint Typhoon Warning Center (JTWC)], the surface horizontal circulation of TC is divided into four cardinal quadrants in space. Quadrant 1, 2, 3, and 4 correspond to the northeast (NE), northwest (NW), southwest (SW), and southeast (SE) quadrants about the TC center, respectively.

Second, the degree of TC size asymmetry (α) is defined as the ratio of the maximum R34 among the 4 quadrants ($R34_{MAX}$) to the effective R34 ($R34_{EFF}$) minus 1:

$$\alpha = \frac{R34_{MAX}}{R34_{EFF}} - 1$$

$$R34_{MAX} = \max\left(R34_{NE}, R34_{NW}, R34_{SW}, R34_{SE}\right)$$

$$R34_{EFF} = \sqrt{\frac{R34_{NE}{}^2 + R34_{NW}{}^2 + R34_{SW}{}^2 + R34_{SE}{}^2}{4}}$$

where the R34, the radius of 10-m gale-force (34-kt) winds from the TC center, is one of the most typical metrics that has been widely used for specifying the outer-core size of TC (Chan and Chan 2018). The α and $R34_{EFF}$ range between 0 and 1, and 0.5 $R34_{MAX}$ and $R34_{MAX}$, respectively. The larger the α, the more asymmetric of the TC size is. At the low end ($\alpha = 0$; $R34_{EFF} = R34_{MAX}$), the R34 of four quadrants are identical ($R34_{NE} = R34_{NW} = R34_{SW} = R34_{SE} = R34_{MAX}$) such that the TC size is axisymmetric. At the high end ($\alpha = 1$; $R34_{EFF} = 0.5\ R34_{MAX}$), there is only one quadrant where $R34 > 0$ such that the TC size is highly asymmetric. The denominator $R34_{EFF}$ is taken as the reference rather than the 4-quadrant mean R34 because it specifies how large the effective areal influence of a TC is, which is more physical and consistent with the concept of TC size (Zhang and Chan 2023).

Third, utilizing the α and $R34_{EFF}$, the asymmetry is categorized into five types (T; Fig. 1). For the cases $\alpha \leq$ critical α ($\alpha \leq \alpha_C = 0.13$), they are categorized as Type O. The cases within such 13% variability are categorized as the quasi-symmetric type. It accounts for 15.03% of the global samples (Fig. 2; Table 1). The α_C is derived from the 41-year TC size climatology (1979–2019; Zhang and Chan 2023) in the Northern Hemisphere (NH) and Southern Hemisphere (SH):

$$\alpha_C = \frac{\max\left(\frac{\overline{R34_{NE,NH}}+\overline{R34_{NE,SH}}}{2}, \frac{\overline{R34_{NW,NH}}+\overline{R34_{NW,SH}}}{2}, \frac{\overline{R34_{SW,NH}}+\overline{R34_{SW,SH}}}{2}, \frac{\overline{R34_{SE,NH}}+\overline{R34_{SE,SH}}}{2}\right)}{\sqrt{\frac{\left(\frac{\overline{R34_{NE,NH}}+\overline{R34_{NE,SH}}}{2}\right)^2+\left(\frac{\overline{R34_{NW,NH}}+\overline{R34_{NW,SH}}}{2}\right)^2+\left(\frac{\overline{R34_{SW,NH}}+\overline{R34_{SW,SH}}}{2}\right)^2+\left(\frac{\overline{R34_{SE,NH}}+\overline{R34_{SE,SH}}}{2}\right)^2}{4}}} - 1$$

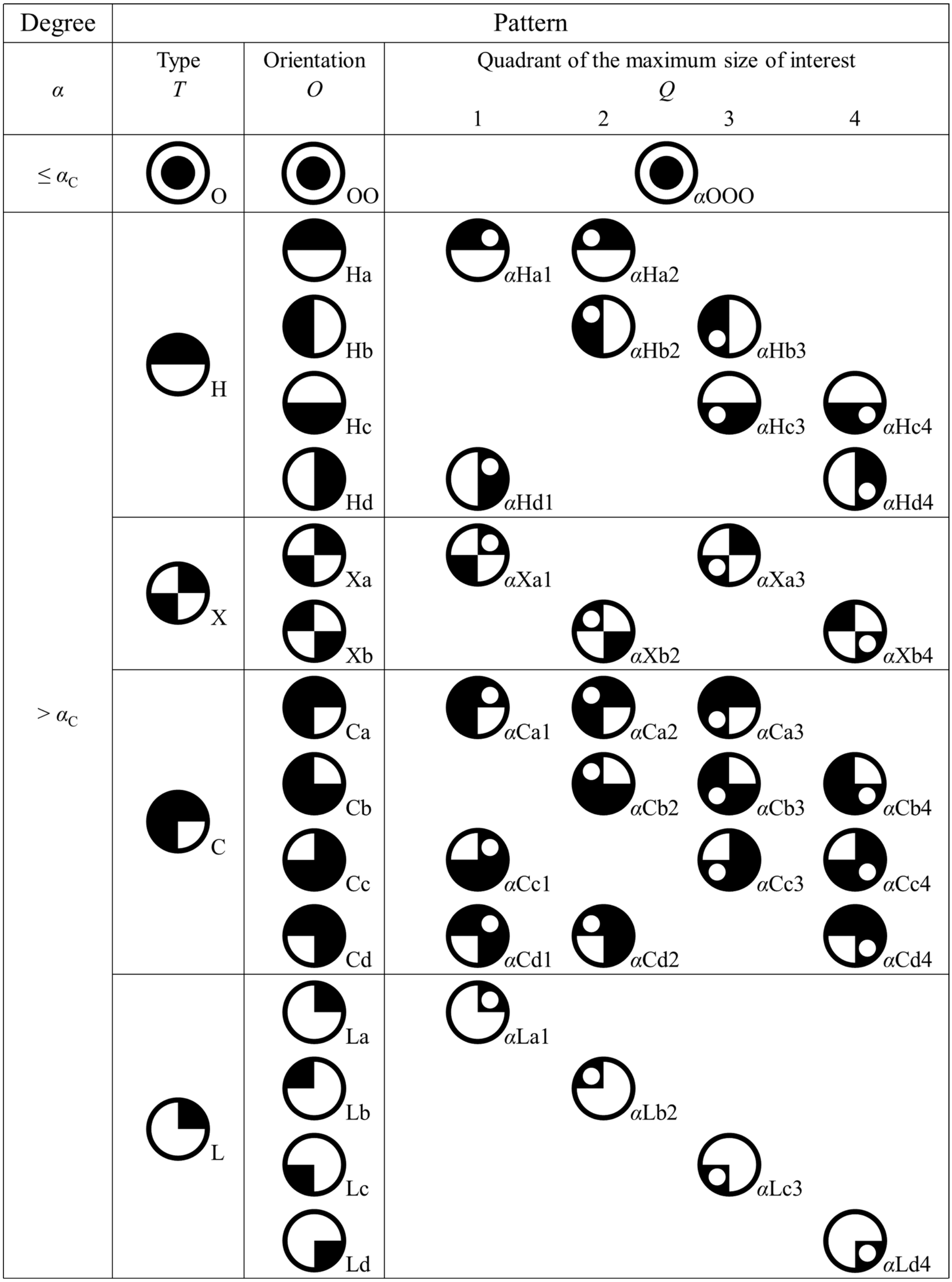

Fig. 1 Ideas and constitutions of SAI. In this study, quadrants in black (white) indicate the corresponding R34 are larger (smaller) than $R34_{EFF}$. Quadrant with white dot specifies the quadrant of $R34_{MAX}$. Distinguishing from the asymmetries in Types H, X, C, and L, the archery target symbol in Type O denotes the TC size which is quasi-symmetric

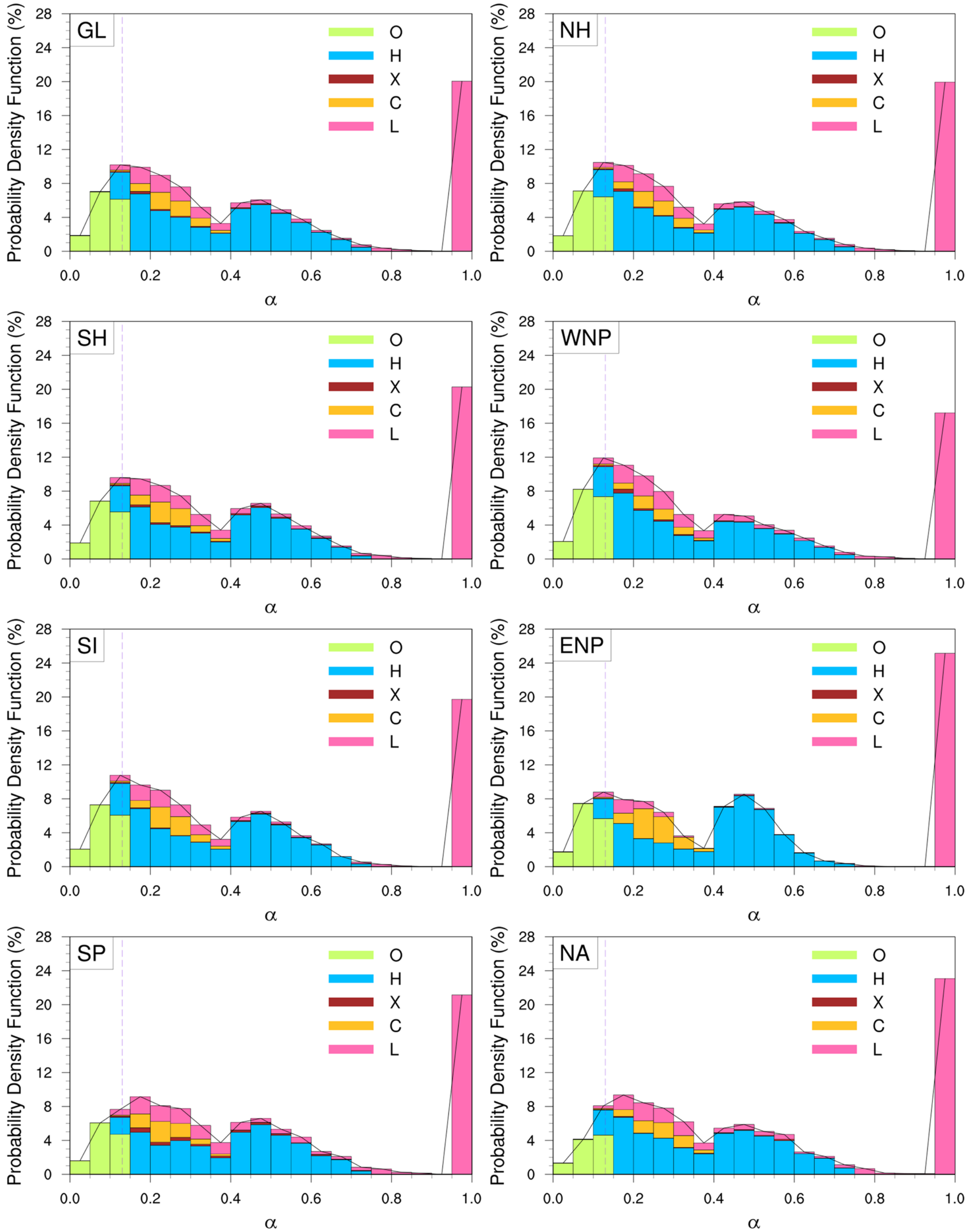

Fig. 2 Global climatological probability density functions of α and T. Climatological probability density functions of α and T in the globe (GL), Northern Hemisphere (NH), Southern Hemisphere (SH), western North Pacific (WNP), South Indian Ocean (SI), eastern North Pacific (ENP), South Pacific (SP), and North Atlantic (NA). The dash vertical reference line indicates the α_C (0.13 in this study)

It assumes the general distributions of atmospheric circulation, temperature, moisture, and planetary vorticity are hemispherically-flipped along the equator, and the circulation of TC is axisymmetric in a quiescent and uniform environment. Taking an average between the NH and SH would therefore largely smooth out the hemispheric-flip and external effects that could contribute to the asymmetry,

Table 1 Climatological statistics of SAI over the western North Pacific (WNP), eastern North Pacific (ENP), North Atlantic (NA), South Indian Ocean (SI), South Pacific (SP), Northern Hemisphere (NH = WNP + NA + ENP), Southern Hemisphere (SH = SI + SP), and globe (GL = NH + SH) in 1979–2019

	WNP	ENP	NA	SI	SP	NH	SH	GL
No. of samples	10,050	2823	4001	4852	3004	16,874	7856	24,730
No. of TCs	768	259	638	402	262	1665	664	2329
α								
Mean	0.41	0.48	0.49	0.44	0.47	0.44	0.45	0.44
Standard deviation	0.31	0.34	0.32	0.32	0.32	0.32	0.32	0.32
25th percentile	0.16	0.20	0.21	0.18	0.20	0.18	0.19	0.18
75th percentile	0.57	1	0.70	0.60	0.65	0.61	0.61	0.61
T (%)								
O	17.64	14.84	10.07	15.44	12.38	15.38	14.27	15.03
H	45.65	45.84	47.84	47.49	43.01	46.20	45.77	46.07
X	1.55	0.32	0.87	0.95	3.03	1.19	1.74	1.36
C	4.76	9.67	6.02	6.90	6.62	5.88	6.80	6.17
L	30.40	29.33	35.19	29.23	34.95	31.36	31.42	31.37
O (%)								
◉	17.64	14.84	10.07	15.44	12.38	15.38	14.27	15.03
◓	14.42	28.27	14.42	5.15	9.39	16.74	6.77	13.57
◐	1.82	0.46	2.87	1.96	3.03	1.84	2.37	2.01
◒	5.75	1.88	10.30	23.95	12.42	6.18	19.54	10.42
◑	23.66	15.23	20.24	16.43	18.18	21.44	17.1	20.06
◍	0.13	0.18	0.07	0.80	2.90	0.12	1.6	0.59
◍	1.42	0.14	0.80	0.14	0.13	1.06	0.14	0.77
◕	0.25	0.74	0.25	1.2	1.33	0.33	1.25	0.62
◕	0.83	0.07	1.35	0.70	0.50	0.82	0.62	0.76
◕	1.04	1.31	1.02	4.23	3.76	1.08	4.05	2.03
◕	2.64	7.55	3.40	0.78	1.03	3.64	0.88	2.76
◔	13.05	20.30	13.87	5.71	15.78	14.46	9.56	12.9
◴	6.35	3.44	6.42	2.12	1.33	5.88	1.82	4.59
◵	0.65	0.53	2.07	6.92	9.89	0.97	8.06	3.22
◶	10.35	5.07	12.82	14.47	7.96	10.05	11.98	10.66
Q (%)								
1	37.11	59.55	38.39	18.30	38.32	41.17	25.95	36.34
2	13.04	9.67	11.35	6.10	5.63	12.08	5.92	10.12
3	2.87	1.81	6.72	15.17	19.61	3.60	16.87	7.82
4	29.33	14.13	33.47	44.99	24.07	27.78	36.99	30.70

and hence, generally remaining the TC circulation and internal forcings themselves. By contrary, for the cases $\alpha > \alpha_C$ (84.97% of the global samples), they are categorized as the asymmetric types: wavenumber-1, wavenumber-2, 3-quarter, and 1-quarter types (Fig. 1). For ease of presentation, they are vividly indexed by the forms of characters H, X, C, and L, respectively.

Fourth, all possible orientations (*O*) in each type are further classified. Types O, H, X, C, and L possess 1, 4, 2, 4, and 4 orientations, respectively. The corresponding orientations and indices are shown in Fig. 1. It is noted that a single indistinguishable orientation is classified in Type O because it is quasi-symmetric. Further classification is ambiguous and not meaningfully necessary.

Finally, integrating all the above elements, the code/text form of SAI is synthetically indexed as

$$\text{SAI} = [\alpha][TOQ]$$

where Q specifies the quadrant of R34_{MAX}, the largest areal influence quadrant where we mostly pay attention to. The first term, α, quantifies the degree of size asymmetry, whereas the second term, TOQ, depicts the pattern of size asymmetry. Again, as Type O is quasi-symmetric, it is ambiguous to specify Q and simply indexed as O (Fig. 1).

Figure 1 shows the full ideas and constitutions of SAI. There are 29 patterns (1 quasi-symmetric and 28 asymmetric patterns) in total. To be more presentable and applicable, a set of symbols is vividly designated correspondingly. For example, the SAI 0.07 ◉, 0.32 ◓, 0.43 ⊕, 0.36 ◕, and 1.00 ◶ are equivalent to 0.07OOO, 0.32Ha1, 0.43Xb2, 0.36Cb3, and 1.00Ld4, respectively. The symbolic form of SAI is clean, intuitive, and powerful that helps the interpretation and documentation in applications and research considerably (see e.g., next sections).

4 Overall climatology

The overall distributions of SAI are summarized in Fig. 2 and Table 1. A 41-year global climatology (1979–2019) evidently shows that the sizes of TCs are often asymmetric in nature. The global mean α is 0.44; the hemispheric mean α in the NH and SH are 0.44 and 0.45, respectively; and the basin mean α in the WNP, ENP, NA, SI, and SP are 0.41, 0.48, 0.49, 0.44, and 0.47, accordingly. They are all $> \alpha_C$. In general, the TCs over NA are the most asymmetric and those over the WNP are the least. Consistent with Zhang and Chan (2023), as the samples in the North Indian Ocean (NI) are too small that are not representative for a climatological study, the TCs over the NI are not included in this study either.

Table 1 shows that the distribution of T is basin independent, while those of O and Q are not. The majority of TC size structure appears in Type H, which accounts for 43.01–47.84% among the basins, followed by Type L (29.23–35.19%), Type O (10.07–17.64%), Type C (4.76–9.67%), and Type X (0.32–3.03%), sequentially. However, the proportions of O and Q are found to be basin dependent suggesting that there should exist interbasin variabilities in dynamics (e.g., basin-dependent monsoon systems, subtropical highs, vertical wind shear, nature of vortex circulations in the NH and SH, etc.) and/or thermodynamics (e.g., basin-dependent moisture transport, dry air intrusions, temperature distributions, etc.). For instance, the largest proportions of O in the WNP, ENP, NA, SI, and SP are ◑, ◓, ◑, ◒, and ◑, followed by ◉, ◔, ◓, ◑, and ◔, correspondingly; and the largest proportions of Q are 1, 1, 1, 4, and 1, followed by 4, 4, 4, 1, and 4, correspondingly. These are largely consistent with Zhang and Chan (2023).

The climatology shows that the α exhibits a trimodal distribution universally (Fig. 2). On global average, the first, second, and third peaks peak at 0.1–0.15, 0.45–0.50, and 1, respectively. The first and second peaks are relatively low and blunt, where the former is higher than the latter. The first peak is the mixture of Type O, H, C, and L TCs, whereas the second peak is largely featured by the Type H TCs. By contrast, the third peak is relatively high and sharp, isolated, and Type L exclusive. Remarkably, on basin average, the distribution in the ENP is distinctly different from those in other basins. Its first and second peaks are comparable and the third peak is the highest. These suggest that the distribution of TC size asymmetry over the ENP is generally less variant. It is likely because (1) the sample size in the ENP is small; and (2) the seasonal variability of subtropical high over the ENP is low such that the ENP TCs are largely confined at low-latitude regions and constrained by similar environment throughout the TC season.

Noticeably, Table 2 shows that about half of the tropical storms are Type L. The proportion of Type L TCs decreases significantly with TC intensity (from 49.88% at intensity of tropical storm to 22.21% at intensity of super typhoon), while that of Type O TCs increases considerably from 3.82 to 22.53%. The corresponding mean α decreases with TC intensity (from 0.67 to 0.30), which agrees with previous studies (Klotz and Jiang 2017; Sun et al. 2019). The correlation coefficient between α and TC intensity is statistically significant at 0.39. Results imply that both the pattern and degree of TC asymmetry are TC intensity dependent. Climatologically, weak TCs are more asymmetric, whereas strong TCs are less asymmetric. It is physical because a weaker TC possesses lower inertial stability to resist perturbations from the environment contributing to the size asymmetry, and vice versa (Liang and Chan 2021).

Previous studies macroscopically suggested that the sizes of slow-moving TCs are less asymmetric, while those of fast-moving TCs are more asymmetric in general (Klotz and Jiang 2017; Olfateh et al. 2017; Tamizi et al. 2020). This statement can also be largely reflected from the present study (Table 2). The mean α increases with TC translation speed (from 0.40 at very slow translation speed to 0.55 at very fast translation speed). However, microscopically, this study reveals that the statement is largely true for the fast-moving TCs, but not the slow-moving TCs. The dependence of TC translation speed on the TC size asymmetry is non-linear. Among the fast-moving TCs, the Type H and Type L TCs dominate (47.46–54.05% and 34.54–41.19%, respectively). The sizes of fast-moving TCs are therefore more asymmetric in general. Nonetheless, among the slow-moving TCs, the proportions of Type O, Type H, and Type L TCs are comparable (22.34–28.28%, 33.65–41.18%, and 27.40–29.02%, respectively). The slow-moving TCs are thus not solely prevailed by the less asymmetric TCs. They can be highly asymmetric either. This implies that when the movement of TC is slow, the factors other than

Table 2 Mean α and proportions of samples (unit: %) in different asymmetric types at different TC intensity (measured by maximum sustained wind speed, V_{MAX}) and translation speeds (M) in 1979–2019

	Category	*n*	Type O	Type H	Type X	Type C	Type L	$\bar{\alpha}$
Intensity V_{MAX} (kt)								
$34 \le V_{MAX} < 48$	Tropical storm	3847	3.82	39.85	1.74	4.70	49.88	0.67
$48 \le V_{MAX} < 64$	Severe tropical storm	5042	8.61	45.82	1.77	6.23	37.58	0.54
$64 \le V_{MAX} < 81$	Typhoon	6186	15.87	47.66	1.20	6.66	28.61	0.43
$81 \le V_{MAX} < 100$	Severe typhoon	3580	21.90	47.09	1.17	6.76	23.07	0.34
$V_{MAX} \ge 100$	Super typhoon	6075	22.53	47.98	1.07	6.21	22.21	0.30
Translation speed M (km h^{-1})								
$M < 8$	Very slow	2719	28.28	33.65	1.03	8.02	29.02	0.40
$8 \le M < 16$	Slow	7722	22.34	41.18	0.73	8.35	27.40	0.40
$16 \le M < 24$	Medium	7685	11.61	51.02	1.12	5.31	30.94	0.44
$24 \le M < 32$	Fast	3671	5.91	54.05	1.61	3.90	34.54	0.50
$M \ge 32$	Very fast	2933	3.85	47.46	3.68	3.82	41.19	0.55

The *n* is the number of samples

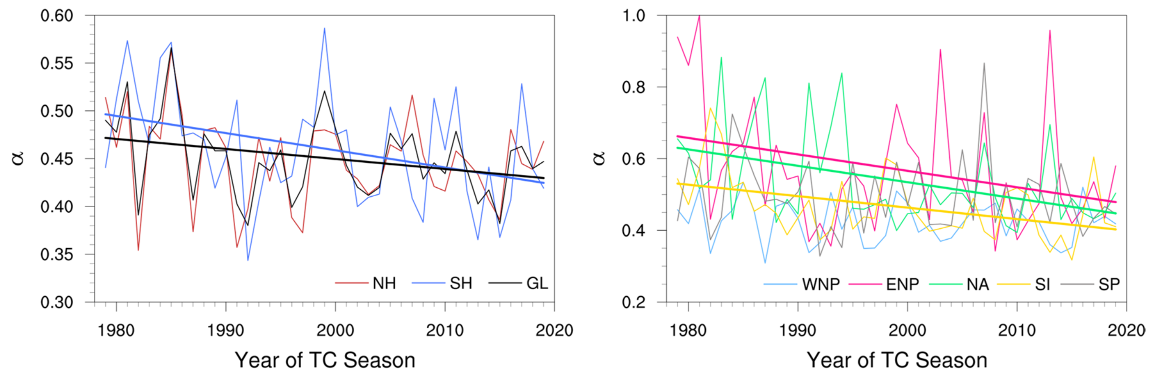

Fig. 3 Time-series and trends of annual mean α in different regions. Only the trends that are statistically significant at the 95% confidence level are shown

the TC translation speed contributing to the size asymmetry become effective.

5 Temporal variations

The interannual variations of α are apparent (Fig. 3). The variabilities are notably larger in the ENP and NA. Meanwhile, the global mean α is found to be significantly decreasing in 1979–2019 (-0.01 decade^{-1}), in which the trends are particularly evident in the ENP (-0.05 decade^{-1}), NA (-0.05 decade^{-1}), and SI (-0.03 decade^{-1}) while those in the WNP and SP are insignificant. However, the reasons for these are not clear. Preliminarily, (1) the α in the WNP is found to have significant negative correlations with the El Niño-Southern Oscillation (ENSO; $r = -0.58$; one of the most important signals of interannual climate variability in the tropics; examined by the contemporaneous July–August–September–October Niño 3.4 index) and the Indian Ocean Basin-Wide Mode (IOBW; $r = -0.38$; examined by the contemporaneous July–August–September–October IOBW index); (2) the α in the ENP shows significant negative correlations with the Arctic Oscillation (AO; $r = -0.35$; examined by the contemporaneous January–February–March–April AO index) and the North Atlantic Oscillation (NAO; $r = -0.33$; examined by the contemporaneous January–February–March–April NAO index); (3) the α in NA has significant correlations with the Atlantic Meridional Mode (AMM; $r = -0.42$; examined by the contemporaneous July–August–September–October AMM index), the Pacific Decadal Oscillation (PDO; $r = 0.33$; examined by the contemporaneous July–August–September–October PDO index), the Atlantic Multidecadal Oscillation (AMO; $r = -0.45$; examined by the contemporaneous July–August–September–October AMO index), and the Southern Annular Mode (SAM; $r = -0.32$; examined by the contemporaneous January–February–March–April SAM index); and (4) the signs of long-term α trends and translation speeds are not fully matched, for example, the translation speeds of NA TCs are increasing over 1970–2016 (Chan 2019) but the corresponding α exhibits the other way round. All these suggest that the interannual variations and trends of α could be a compound of various factors which require future investigations.

In addition, the seasonal variations of α are remarkable (Fig. 4). The α generally decreases from the early summer, reaches the minimum in the fall, and then rebounds. It is partly because (1) more Type H and Type L TCs are in early and late TC season; and (2) the intensity of TCs is generally stronger in mid-to-late TC season such that more Type O TCs appear in the late summer and early fall agreeing the aforementioned inertial stability concept. It is noted that the monthly TC translation speed is weakly correlated with the monthly α (not shown). To comprehend the spatial variations with season in detail, the spatiotemporal variations of *TOQ* are examined next.

6 Spatiotemporal variations

The global climatological spatiotemporal distributions show that the TC size asymmetry patterns *TOQ* vary with time and space (Figs. 5, 6, 7 and 8). Their seasonal, intrabasin, and interbasin variations are apparent. The proportions of asymmetric types are observed not evenly distributed along the TC season, within the basin, and across basins. In this study, the main TC season from July to October in the NH and that from January to April in the SH are investigated.

In the ENP, ◓ and ◔ prevail in early TC season (◓ and ◷ in particular), and more ◑ and ◶ appear at higher latitudes (◑ and ◶ in particular) from mid to late season gradually. Type X TCs are rare throughout the TC season. In the WNP and NA, the main orientation of Type H TCs transits from ◓ at low latitudes to ◑ and ◒ at higher latitudes, while that of Type L TCs transits from ◔ to ◶ correspondingly. These could be probably attributed to the TC track or movement, that is, the superposition of the large-scale subtropical high-driven steering and the TC circulation itself. The west-northwestward steering at low latitudes and the northward-to-northeastward steering under TC recurvature at higher latitudes could lead to these asymmetries.

Comparing to those in the NH, the spatiotemporal distributions of size asymmetry patterns are more diverse in the SH, especially in SP. Type X TCs are slightly more in the SH. The main orientations of asymmetry are ◒ and ◑, which are north-south flipped from those in the NH.

In addition, the proportions of Type O TCs are found to increase broadly along the TC season. This suggests that the aforementioned seasonal increases in Type O TCs (Fig. 4) are not featured by the small regional scale increases in Type O TCs, but the basin-wide or worldwide increases. This could be related to the large-scale seasonal variability. Meanwhile, the occurrence of Type O TCs becomes more scattered along the TC season over NA. Furthermore, it is notable that the $R34_{MAX}$ generally appears in quadrants 1 and 4 globally. More than 60% of Q are found in these two quadrants (Table 1). In particular, for Type L, the majority of Q does not change from July to September in some regions (e.g., 15–30° N, 135–150° E) where ◷ is the commonest. These could be related to the intrinsic properties of TC itself, self-rotating earth, or regional environmental factor(s).

More investigations are needed to consolidate, advance, and understand the above climatology. Note that the size asymmetry variation in synoptic time scale is also evident (not shown) and will be explicitly examined based on the SAI framework in future studies.

7 Conclusions and discussion

A novel TC size asymmetry index (SAI) is proposed to specify the degree and pattern of TC size asymmetry synthetically. It provides an additional metric that effectively describes the horizontal damaging wind distribution of a TC. It is practically essential, intuitive, and useful for interpretation and documentation in application and research fields. A 41-year global climatology (1979–2019) and the power of SAI are elementarily revealed and demonstrated. The distribution of the degree of TC size asymmetry is trimodal. The size asymmetry of TC is found to be TC intensity, TC movement, time, and space dependent. In general, the weak or fast-moving TCs are more asymmetric. The interannual variations and long-term trends of α could be a compound of various factors. The seasonal variation of α generally decreases from the early summer, reaches the minimum in the fall, and then rebounds. The proportions of asymmetric types are not evenly distributed along the TC season, within the basin, and across basins.

This study serves as an introduction and promotion of SAI which lays an important foundation for future applications and research. The in-depth examinations of TC size asymmetry in each basin utilizing SAI are effectively meaningful. The corresponding underlying factors/mechanisms leading to long-term trends and different patterns of TC size asymmetry (especially the changes in synoptic time scale) are warranted. All these form a series of follow-ups which are on-going stepwise. Enlighteningly, besides meteorology, this work could inspire other fields to index or specify the geometric asymmetries of other kinds.

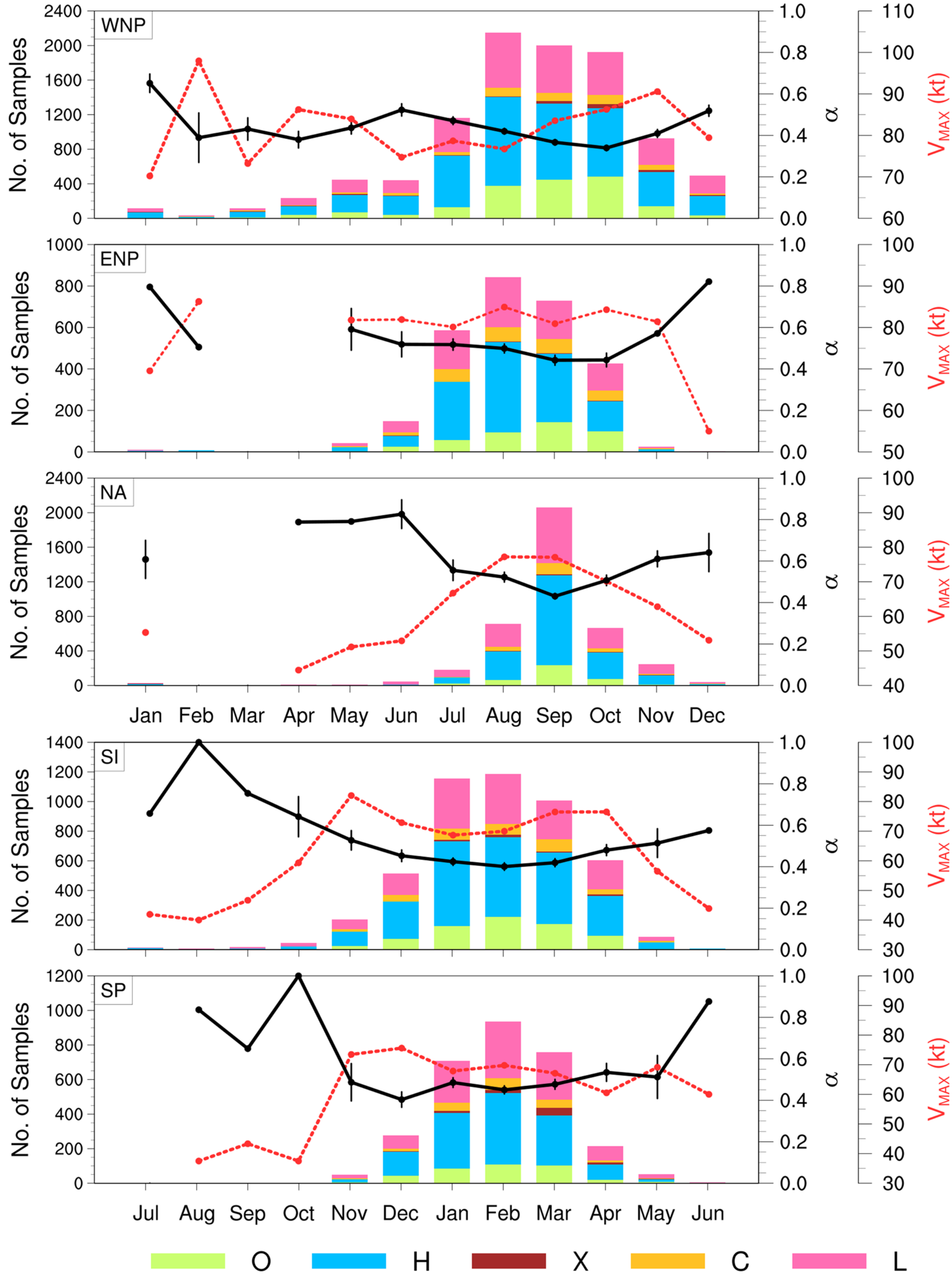

Fig. 4 Time series of monthly mean α and V_{MAX} in different basins. The bars indicate the corresponding numbers of samples with T specified. The ranges of each α data point represent the 95% confidence intervals in the t distribution (only the data points with number of samples ≥ 30 are shown). Note that the x-axes start from the hemispheric winter

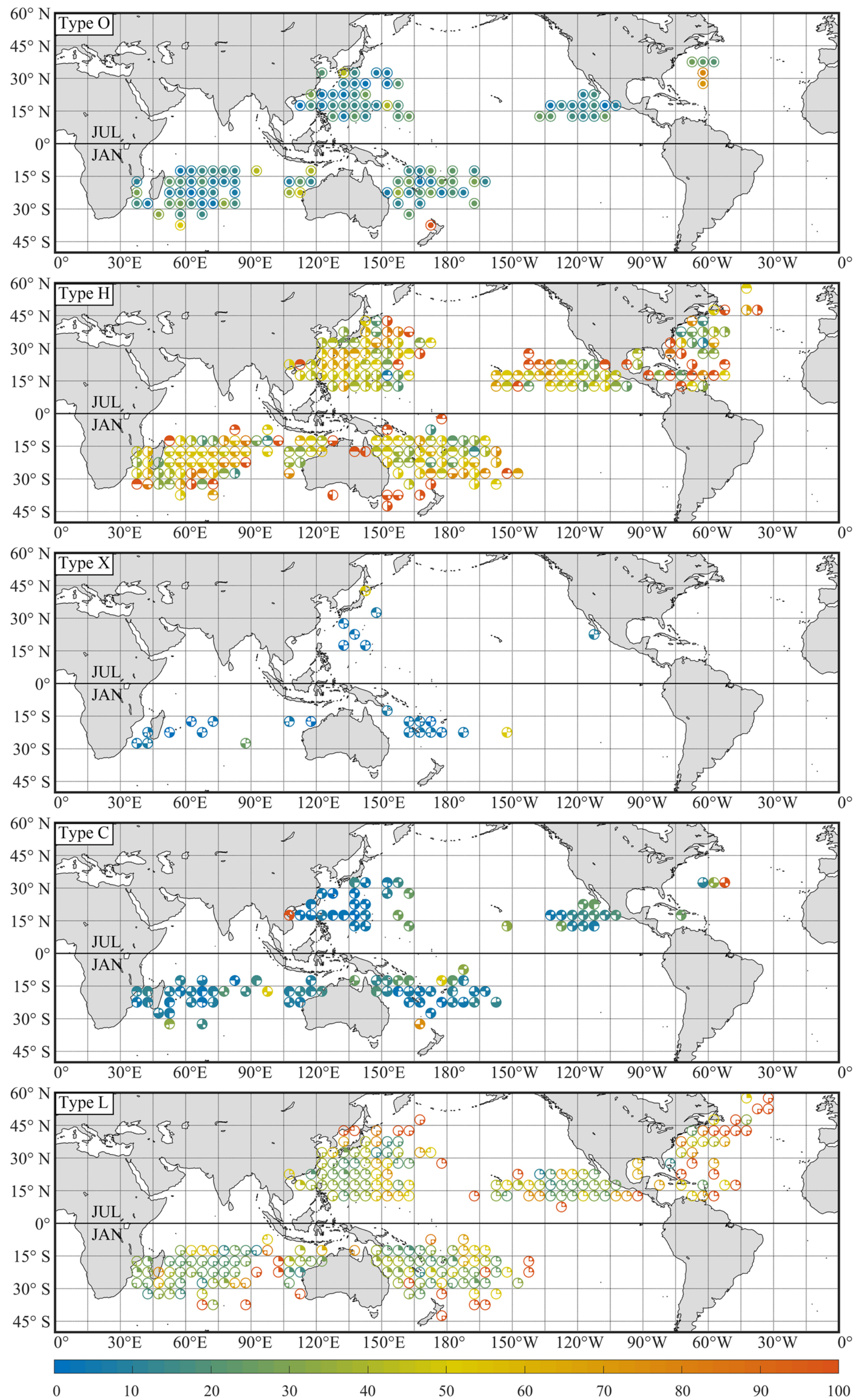

Fig. 5 Global climatological spatiotemporal distributions of *TOQ* in NH July and SH January. In each *T*, the most corresponding prominent *TOQ* in each 5° latitude × 5° longitude grid is shown by the corresponding symbol. The colour of symbol depicts the proportion (unit: %) of the corresponding *T* within the grid. Note that when there are two or more *TOQ* sharing the same maximum proportion in the same grid, only the corresponding *T* symbol is shown

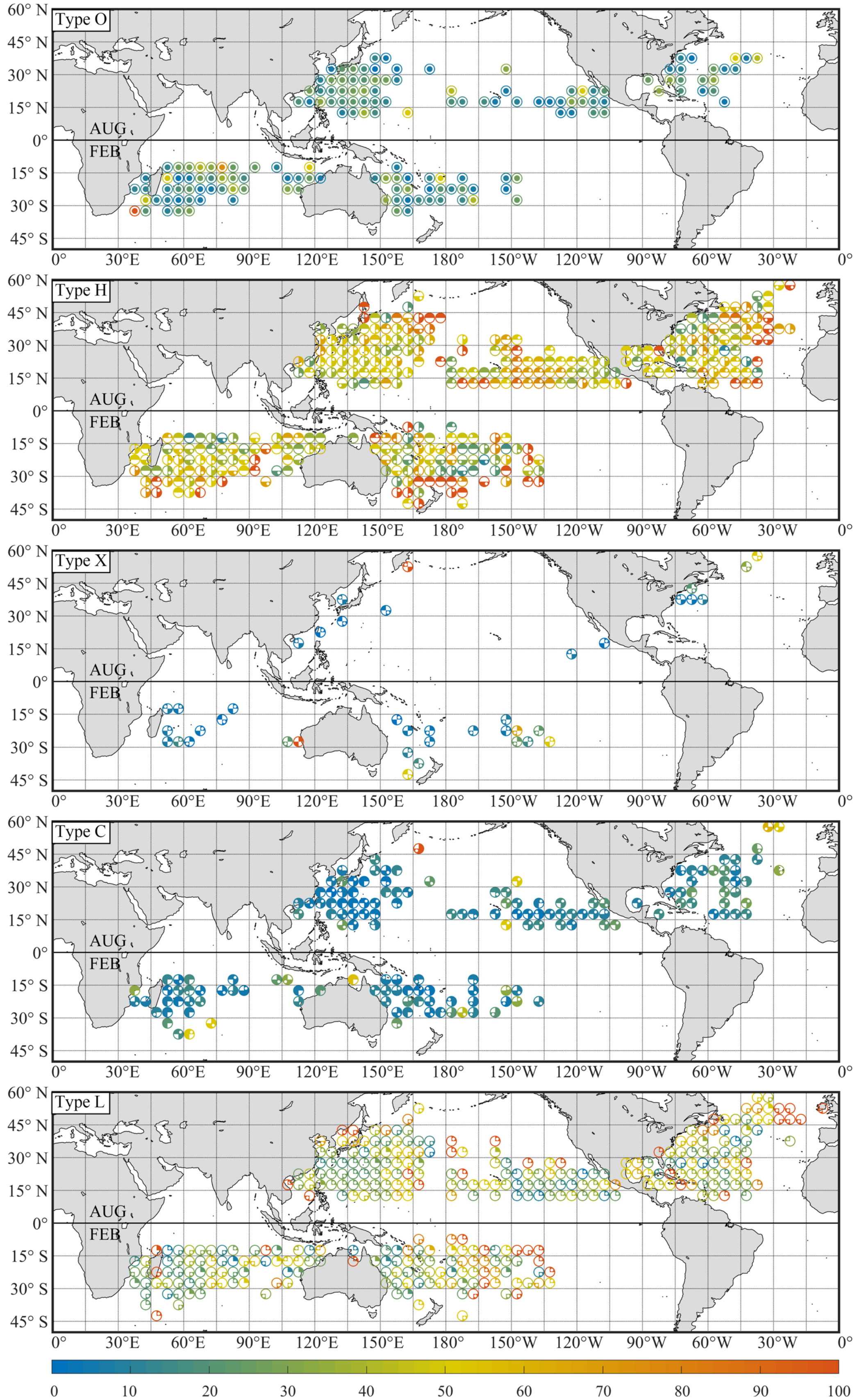

Fig. 6 As in Fig. 5, but in NH August and SH February

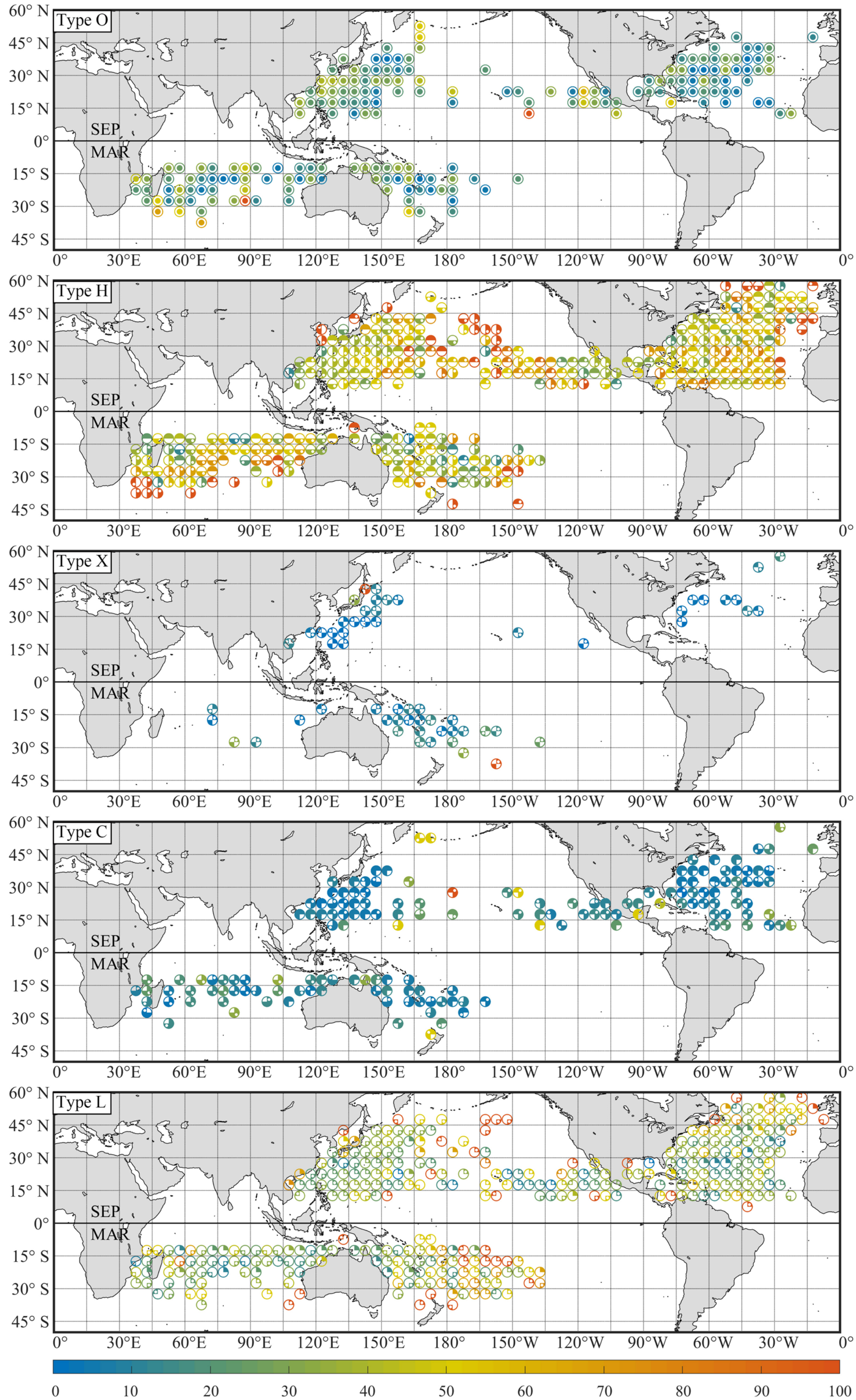

Fig. 7 As in Fig. 5, but in NH September and SH March

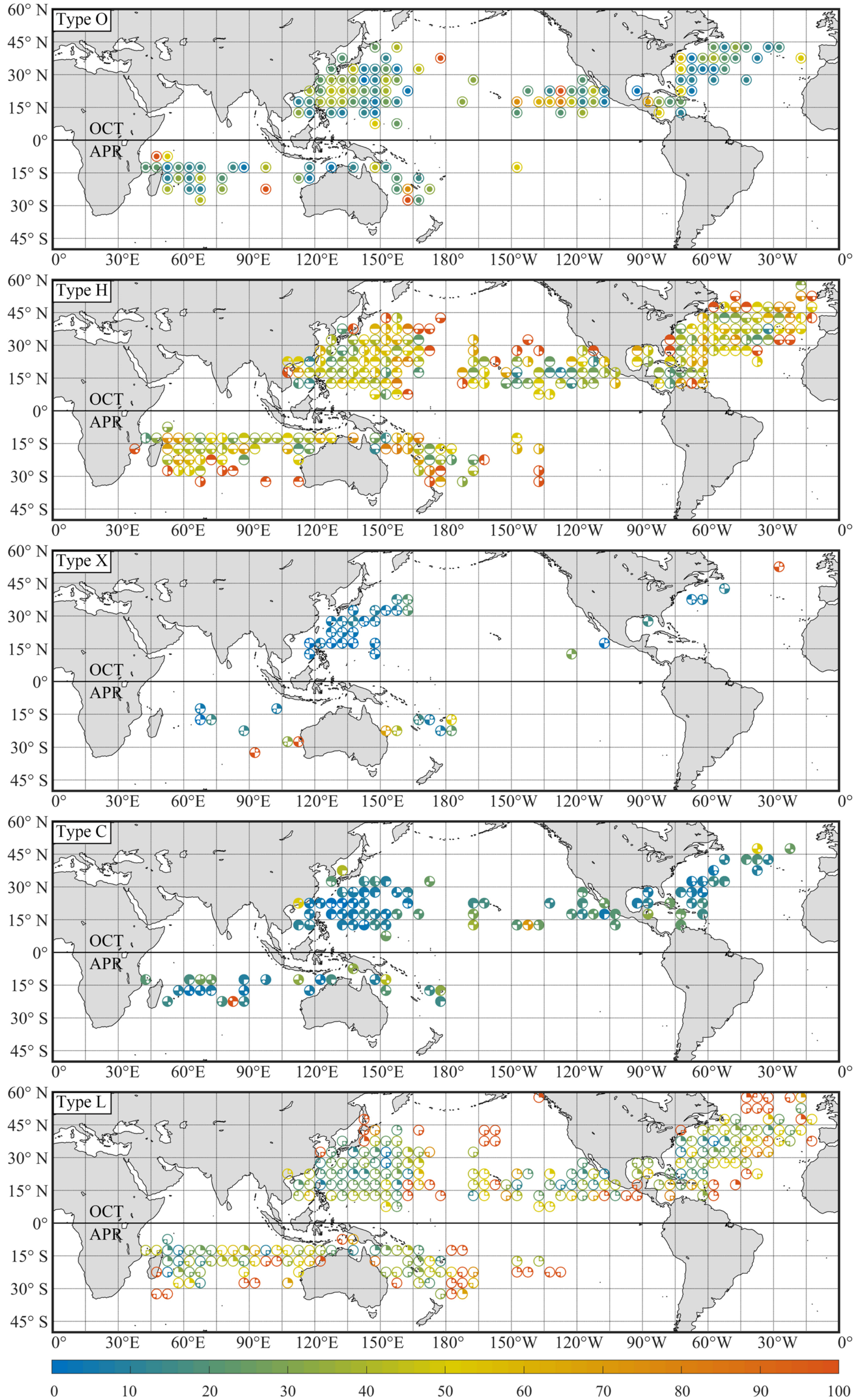

Fig. 8 As in Fig. 5, but in NH October and SH April

Table 3 KTFCHAN font table

Order	Symbol	Description	Input character	Unicode name
1		Blank space		Space
2	◉	SAI: O, OO, OOO	!	Exclamation mark
3		SAI: H, Ha	“	Quotation mark
4		SAI: Ha1	#	Number sign
5		SAI: Ha2	$	Dollar sign
6		SAI: Hb	%	Percent sign
7		SAI: Hb2	&	Ampersand
8		SAI: Hb3	‘	Apostrophe
9		SAI: Hc	(	Left parenthesis
10		SAI: Hc3	)	Right parenthesis
11		SAI: Hc4	*	Asterisk
12		SAI: Hd	+	Plus sign
13		SAI: Hd1	,	Comma
14		SAI: Hd4	-	Hyphen-minus
15		SAI: X, Xa	.	Full stop
16		SAI: Xa1	/	Solidus
17		SAI: Xa3	0	Digit zero
18		SAI: Xb	1	Digit one
19		SAI: Xb2	2	Digit two
20		SAI: Xb4	3	Digit three
21		SAI: C, Ca	4	Digit four
22		SAI: Ca1	5	Digit five
23		SAI: Ca2	6	Digit size
24		SAI: Ca3	7	Digit seven
25		SAI: Cb	8	Digit eight
26		SAI: Cb2	9	Digit nine
27		SAI: Cb3	:	Colon
28		SAI: Cb4	;	Semicolon
29		SAI: Cc	<	Less-than sign
30		SAI: Cc1	=	Equal sign
31		SAI: Cc3	>	Greater-than sign
32		SAI: Cc4	?	Question mark
33		SAI: Cd	@	Commercial at
34		SAI: Cd1	A	Latin capital letter A
35		SAI: Cd2	B	Latin capital letter B
36		SAI: Cd4	C	Latin capital letter C
37		SAI: L, La	D	Latin capital letter D
38		SAI: La1	E	Latin capital letter E
39		SAI: Lb	F	Latin capital letter F
40		SAI: Lb2	G	Latin capital letter G
41		SAI: Lc	H	Latin capital letter H
42		SAI: Lc3	I	Latin capital letter I
43		SAI: Ld	J	Latin capital letter J
44		SAI: Ld4	K	Latin capital letter K
45	○	White circle	L	Latin capital letter L
46	●	Black circle	M	Latin capital letter M
47		Northern Hemisphere cyclone	N	Latin capital letter N
48		Southern Hemisphere cyclone	O	Latin capital letter O

For popularization and accessibility, a dedicated font KTFCHAN in formats of OpenType Font (OTF), TrueType Font (TTF), Web Open Font Format version 1 (WOFF), and Web Open Font Format version 2 (WOFF2) are developed, published, and available in Supplementary Information. The details of font are given in Table 3. They are free to download and install. Any commercial use is prohibited. All rights are reserved by Kelvin T. F. Chan. Recommendations for adding other symbols to the font are welcome upon reasonable request. The SAI has been incorporated in the database established by Zhang and Chan (2023) which is also available in Supplementary Information.

Supplementary Information The online version contains supplementary material available at https://doi.org/10.1007/s00382-023-06840-5.

Author contributions KTFC conceived the idea, performed the analyses, wrote the manuscript, and established the KTFCHAN font. KZ and LX performed the analyses. All authors contributed to the discussion.

Funding This study was supported by the National Key R&D Program of China (2019YFC1510400), the National Natural Science Foundation of China (41975052), the Guangdong Basic and Applied Basic Research Foundation (2023A1515010741), the Innovation Group Project of the Southern Marine Science and Engineering Guangdong Laboratory (Zhuhai) (311021001), and the Guangdong Province Key Laboratory for Climate Change and Natural Disaster Studies (2020B1212060025).

Data availability The ERA5-derived global TC size database is available at Zhang and Chan (2023). The Niño 3.4 index is extracted at https://psl.noaa.gov/gcos_wgsp/Timeseries/Nino34/. The AMM index is obtained at https://psl.noaa.gov/data/timeseries/monthly/AMM/. The NAO index is retrieved at https://psl.noaa.gov/gcos_wgsp/Timeseries/NAO/. The AO index is available at https://psl.noaa.gov/gcos_wgsp/Timeseries/AO/. The PDO index is extracted at https://psl.noaa.gov/gcos_wgsp/Timeseries/PDO/. The AMO index is obtained at https://psl.noaa.gov/data/correlation/. The IOBW index is retrieved at http://cmdp.ncc-cma.net/Monitoring/cn_nino_index.php?product=cn_nino_index_iobw. The SAM index is extracted at https://climatedataguide.ucar.edu/climate-data/marshall-southern-annular-mode-sam-index-station-based. Data that supports the findings of this study is available in Supplementary Information or from the corresponding author on request.

Declarations

Conflict of interest The authors declare no competing interests.

Significance statement Size of tropical cyclone is often asymmetric in nature, but there is a lack of systematic, clean, and intuitive metric to specify the asymmetry which is strongly urged. A novel size asymmetry index (SAI) is therefore proposed to specify both the degree and pattern of asymmetry synthetically in this study. It is practically useful for assessing and expressing the size structure of tropical cyclone, especially for the parties in applications and research.

References

Bian G-F, Nie G-Z, Qiu X (2021) How well is outer tropical cyclone size represented in the ERA5 reanalysis dataset? Atmos Res 249:105339. https://doi.org/10.1016/j.atmosres.2020.105339

Chan KTF (2019) Are global tropical cyclones moving slower in a warming climate? Environ Res Lett 14:104015. https://doi.org/10.1088/1748-9326/ab4031

Chan KTF, Chan JCL (2012) Size and strength of tropical cyclones as inferred from QuikSCAT data. Mon Weather Rev 140:811–824. https://doi.org/10.1175/MWR-D-10-05062.1

Chan KTF, Chan JCL (2013) Angular momentum transports and synoptic flow patterns associated with tropical cyclone size change. Mon Weather Rev 141:3985–4007. https://doi.org/10.1175/MWR-D-12-00204.1

Chan KTF, Chan JCL (2014) Impacts of initial vortex size and planetary vorticity on tropical cyclone size. Q J R Meteorol Soc 140:2235–2248. https://doi.org/10.1002/qj.2292

Chan KTF, Chan JCL (2015a) Global climatology of tropical cyclone size as inferred from QuikSCAT data. Int J Climatol 35:4843–4848. https://doi.org/10.1002/joc.4307

Chan KTF, Chan JCL (2015b) Impacts of vortex intensity and outer winds on tropical cyclone size. Q J R Meteorol Soc 141:525–537. https://doi.org/10.1002/qj.2374

Chan KTF, Chan JCL (2016) Sensitivity of the simulation of tropical cyclone size to microphysics schemes. Adv Atmos Sci 33:1024–1035. https://doi.org/10.1007/s00376-016-5183-2

Chan KTF, Chan JCL (2018) The outer-core wind structure of tropical cyclones. J Meteorol Soc Jpn 96:297–315. https://doi.org/10.2151/jmsj.2018-042

Chan KTF, Zhang K, Wu Y, Chan JCL (2022a) Landfalling hurricane track modes and decay. Nature 606:E7–E11. https://doi.org/10.1038/s41586-022-04791-1

Chan KTF, Chan JCL, Zhang K, Wu Y (2022b) Uncertainties in tropical cyclone landfall decay. NPJ Clim Atmos Sci 5:93. https://doi.org/10.1038/s41612-022-00320-z

Chavas DR, Emanuel KA (2010) A QuikSCAT climatology of tropical cyclone size. Geophys Res Lett 37:L18816. https://doi.org/10.1029/2010GL044558

Chavas DR, Emanuel KA (2014) Equilibrium tropical cyclone size in an idealized state of axisymmetric radiative–convective equilibrium. J Atmos Sci 71:1663–1680. https://doi.org/10.1175/JAS-D-13-0155.1

Chavas DR, Lin N, Dong W, Lin Y (2016) Observed tropical cyclone size revisited. J Clim 29:2923–2939. https://doi.org/10.1175/JCLI-D-15-0731.1

Chen K, Chen G, Rao C, Wang Z (2021) Relationship of tropical cyclone size change rate with size and intensity over the western North Pacific. Atmos Oceanic Sci Lett 14:100040. https://doi.org/10.1016/j.aosl.2021.100040

Dean L, Emanuel KA, Chavas DR (2009) On the size distribution of Atlantic tropical cyclones. Geophys Res Lett 36:L14803. https://doi.org/10.1029/2009GL039051

Hersbach H, Bell B, Berrisford P, Hirahara S, Horanyi A, Munoz-Sabater J, Nicolas J, Peubey C, Radu R, Schepers D, Simmons A, Soci C, Abdalla S, Abellan X, Balsamo G, Bechtold P, Biavati G, Bidlot J, Bonavita M, De Chiara G, Dahlgren P, Dee D, Diamantakis M, Dragani R, Flemming J, Forbes R, Fuentes M, Geer A, Haimberger L, Healy S, Hogan RJ, Holm E, Janiskova M, Keeley S, Laloyaux P, Lopez P, Lupu C, Radnoti G, De Rosnay P, Rozum I, Vamborg F, Villaume S, Thepaut JN (2022) The ERA5 global reanalysis. Q J R Meteorol Soc 146:1999–2049. https://doi.org/10.1002/qj.3803

Hill KA, Lackmann GM (2009) Influence of environmental humidity on tropical cyclone size. Mon Weather Rev 137:3294–3315. https://doi.org/10.1175/2009MWR2679.1

Hong W, Zheng Y, Chen B, Su T, Ke X (2020) Monthly variation and spatial distribution of quadrant tropical cyclone size in the western North Pacific. Atmos Sci Lett 21:e956. https://doi.org/10.1002/asl.956

Irish JL, Resio DT, Ratcliff JJ (2008) The influence of storm size on hurricane surge. J Phys Oceanogr 38:2003–2013. https://doi.org/10.1175/2008JPO3727.1

Kim H-J, Moon I-J, Oh I (2022) Comparison of tropical cyclone wind radius estimates between the KMA, RSMC Tokyo, and JTWC. Asia-Pac J Atmos Sci 58:563–576. https://doi.org/10.1007/s13143-022-00274-5

Kimball SK, Mulekar MS (2004) A 15-year climatology of North Atlantic tropical cyclones. Part I: size parameters. J Clim 17:3555–3575. https://doi.org/10.1175/1520-0442(2004)017%3c3555:AYCONA%3e2.0.CO;2

Klotz BW, Jiang H (2016) Global composites of surface wind speeds in tropical cyclones based on a 12 year scatterometer database. Geophys Res Lett 43:10480–10488. https://doi.org/10.1002/2016GL071066

Klotz BW, Jiang H (2017) Examination of surface wind asymmetries in tropical cyclones. Part I: general structure and wind shear impacts. Mon Weather Rev 145:3989–4009. https://doi.org/10.1175/MWR-D-17-0019.1

Knaff JA, DeMaria M, Molenar DA, Sampson CR, Seybold MG (2011) An automated, objective, multiple-satellite-platform tropical cyclone surface wind analysis. J Appl Meteorol Climatol 50:2149–2166. https://doi.org/10.1175/2011JAMC2673.1

Knaff JA, Longmore SP, Molenar DA (2014) An objective satellite-based tropical cyclone size climatology. J Clim 27:455–476. https://doi.org/10.1175/JCLI-D-13-00096.1

Liang J, Chan KTF (2021) Rainfall asymmetries of the western North Pacific tropical cyclones as inferred from GPM. Int J Climatol 41:5465–5480. https://doi.org/10.1002/joc.7136

Lin N, Lane P, Emanuel KA, Sullivan RM, Donnelly JP (2014) Heightened hurricane surge risk in northwest Florida revealed from climatological-hydrodynamic modeling and paleorecord reconstruction. J Geophys Res 119:8606–8623. https://doi.org/10.1002/2014JD021584

Liu KS, Chan JCL (1999) Size of tropical cyclones as inferred from ERS-1 and ERS-2 data. Mon Weather Rev 127:2992–3001. https://doi.org/10.1175/1520-0493(1999)127%3c2992:SOTCAI%3e2.0.CO;2

Liu KS, Chan JCL (2002) Synoptic flow patterns associated with small and large tropical cyclones over the western North Pacific. Mon Weather Rev 130:2134–2142. https://doi.org/10.1175/1520-0493(2002)130%3c2134:SFPAWS%3e2.0.CO;2

Lu K, Chavas D (2022) Tropical cyclone size is strongly limited by the Rhines scale: experiments with a barotropic model. J Atmos Sci 79:2109–2124. https://doi.org/10.1175/JAS-D-21-0224.1

McCaul EW Jr (1991) Buoyancy and shear characteristics of hurricane-tornado environments. Mon Weather Rev 119:1954–1978. https://doi.org/10.1175/1520-0493(1991)119%3c1954:BASCOH%3e2.0.CO;2

Mok DKH, Chan JCL, Chan KTF (2018) A 31-year climatology of tropical cyclone size from the NCEP Climate Forecast System Reanalysis. Int J Climatol 38:e796–e806. https://doi.org/10.1002/joc.5407

Olfateh M, Callaghan DP, Nielsen P, Baldock TE (2017) Tropical cyclone wind field asymmetry—development and evaluation of a new parametric model. J Geophys Res Oceans 122:458–469. https://doi.org/10.1002/2016JC012237

Paredes M, Schenkel BA, Edwards R, Coniglio M (2021) Tropical cyclone outer size impacts the number and location of tornadoes. Geophys Res Lett 48:e2021GL095922. https://doi.org/10.1029/2021GL095922

Schenkel BA, Lin N, Chavas D, Oppenheimer M, Brammer A (2017) Evaluating outer tropical cyclone size in reanalysis datasets using QuikSCAT data. J Clim 30:8745–8762. https://doi.org/10.1175/JCLI-D-17-0122.1

Schenkel BA, Lin N, Chavas D, Vecchi GA, Oppenheimer M, Brammer A (2018) Lifetime evolution of outer tropical cyclone size and structure as diagnosed from reanalysis and climate model data. J Clim 31:7985–8004. https://doi.org/10.1175/JCLI-D-17-0630.1

Song J, Duan Y, Klotzbach PJ (2020) Revisiting the relationship between tropical cyclone size and intensity over the western North Pacific. Geophys Res Lett 47:e2020GL088217. https://doi.org/10.1029/2020GL088217

Song J, Klotzbach PJ (2016) Wind structure discrepancies between two best track datasets for western North Pacific tropical cyclones. Mon Weather Rev 144:4533–4551. https://doi.org/10.1175/MWR-D-16-0163.1

Sun Z, Zhang B, Zhang JA, Perrie W (2019) Examination of surface wind asymmetry in tropical cyclones over the Northwest Pacific Ocean using SMAP observations. Remote Sens 11:2604. https://doi.org/10.3390/rs11222604

Tamizi A, Young IR, Ribal A, Alves JH (2020) Global scatterometer observations of the structure of tropical cyclone wind fields. Mon Weather Rev 148:4673–4692. https://doi.org/10.1175/MWR-D-20-0196.1

Wang S, Toumi R (2019) Impact of dry midlevel air on the tropical cyclone outer circulation. J Atmos Sci 76:1809–1826. https://doi.org/10.1175/JAS-D-18-0302.1

Wang S, Toumi R (2022) An analytic model of the tropical cyclone outer size. NPJ Clim Atmos Sci 5:46. https://doi.org/10.1038/s41612-022-00270-6

Wang S, Toumi R, Czaja A, Kan AV (2015) An analytic model of tropical cyclone wind profiles. Q J R Meteorol Soc 141:3018–3029. https://doi.org/10.1002/qj.2586

Wang S, Lin N, Gori A (2022) Investigation of tropical cyclone wind models with application to storm tide simulations. J Geophys Res Atmos 127:e2021JD036359. https://doi.org/10.1029/2021JD036359

Xu J, Wang Y (2010a) Sensitivity of the simulated tropical cyclone inner-core size to the initial vortex size. Mon Weather Rev 138:4135–4157. https://doi.org/10.1175/2010MWR3335.1

Xu J, Wang Y (2010b) Sensitivity of tropical cyclone inner-core size and intensity to the radial distribution of surface entropy flux. J Atmos Sci 67:1831–1852. https://doi.org/10.1175/2010JAS3387.1

Yang N, Li Y, Chan JCL, Cheung KKW, Ye L, Wu Y (2022) Vertical variation of tropical cyclone size in the western North Pacific. Int J Climatol 42:4424–4444. https://doi.org/10.1002/joc.7477

Yuan J, Wang D, Wan Q, Liu C (2007) A 28-year climatological analysis of size parameters for northwestern Pacific tropical cyclones. Adv Atmos Sci 24:24–34. https://doi.org/10.1007/s00376-007-0024-y

Zhang K, Chan KTF (2023) An ERA5 global climatology of tropical cyclone size asymmetry. Int J Climatol 43:950–963. https://doi.org/10.1002/joc.7846

Zhuo J, Tan Z (2021) Physics-augmented deep learning to improve tropical cyclone intensity and size estimation from satellite imagery. Mon Weather Rev 149:2097–2113. https://doi.org/10.1175/MWR-D-20-0333.1